Springer

KSME

Journal of Mechanical Science and Technology 33 (8) (2019) 4039~4045
www.springerlink.com/content/1738-494x(Print)/1976-3824(Online)
DOI 10.1007/s12206-019-0749-4

Piezoelectric energy harvester utilizing mandibular deformation to power implantable biosystems: A feasibility study †

Richard Fan[1], Soobum Lee[1,*], Hyunjun Jung[1], Mary Anne Melo[2] and Radi Masri[2]

[1]*Department of Mechanical Engineering, University of Maryland, Baltimore County, Baltimore, USA*
[2]*School of Dentistry, University of Maryland, Baltimore, USA*

(Manuscript Received November 29, 2018; Revised April 10, 2019; Accepted May 1, 2019)

Abstract

This study explores the feasibility of energy harvesting from the deformation of a piezoelectric material attached on the human mandible to power an implantable medical device such as deep brain stimulator. A finite element (FE) model of the human mandible was developed and verified experimentally. A piezoelectric energy harvesting device was designed and fixed onto a synthetic mandible to compare its experimental power output to the simulation results. A novel mandibular loading apparatus was designed to imitate the forces exerted on a mandible during mastication in a lab environment. The peak-to-peak voltages from finite element analysis (FEA) and experiment were 1.7 and 1.0 V. Despite the discrepancy in magnitude, similar voltage waveforms were obtained. A method to maximize the electrical efficiency of the proposed harvesting device was discussed.

Keywords: Deep brain stimulation (DBS); Energy harvesting; Mandible; Mastication; Implant; Piezoelectricity

1. Introduction

Deep brain stimulation (DBS) is a surgical procedure that aims to provide therapeutic effects for patients that suffer from various neurological disorders [1]. The implantation procedure of a DBS device is not without morbidity due to the large size of the generator and wiring. Moreover, its limited battery life (on average 3 years [2]) requires additional surgical procedures for battery replacement. There is significant motivation to reduce the number of battery replacements to improve patient quality of life. One potential solution is a self-charging DBS device utilizing energy from the human mandible. Recently, researchers have investigated sources of energy inside the human body to power implantable devices, such as the human heartbeat [3, 4], muscle contractions [5-7] and blood flow [8, 9]. An energy harvester for self-powered DBS has been studied [10], but it did not provide a human application. An energy harvesting rectenna capable of self-powering a DBS system was also designed, but it requires a constant external microwave source [11]. Researchers have also looked towards harvesting energy from cerebrospinal fluid pressure fluctuations, but it is unable to generate practical power for a DBS system (0.62 nW) [12]. An external head-mounted device that harvests energy from jaw movements via a piezoelectric harvester strapped to a human chin was also developed that could possibly power small-scale electronics [13], but is not practical for an in-vivo application. The objective of this paper was to investigate the feasibility of harvesting energy from a similarly flexible piezoelectric energy harvester surgically implanted to the human mandible to power a DBS system. The deformation of the human mandible and the electrical energy generation was investigated, and the piezoelectric harvester mounted on the human mandible was analyzed via finite element analysis and experimentally tested.

2. Finite element analysis of mandible

As the first step of this study, the finite element (FE) model for human mandible was verified via finite element analysis. The finite element mesh of the human mandible used in this paper was obtained from a CT scan of a human cadaver [14]. A mandible's material properties are known to be anisotropic and changing over time [15-17] and different locally [14]. However, it is acceptable to assign linearly isotropic [18] or transversely isotropic [19] properties for the cortical and trabecular bone. In this study, isotropic behavior was assumed for the trabecular bone (red in Fig. 1), cortical bone (purple), and dentin (cyan). A half-model of the mandible was implemented to reduce computation time.

*Corresponding author. Tel.: +1 410 455 3314, Fax.: +1 410 455 1052
E-mail address: sblee@umbc.edu
† Recommended by Associate Editor Won Hyoung Ryu
© KSME & Springer 2019

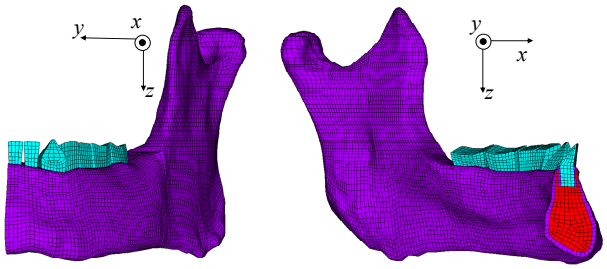

Fig. 1. Frontal (left) and lateral (right) view of the FE model generated from the geometry of a human cadaver- trabecular bone (red); cortical bone (purple); dentin (cyan).

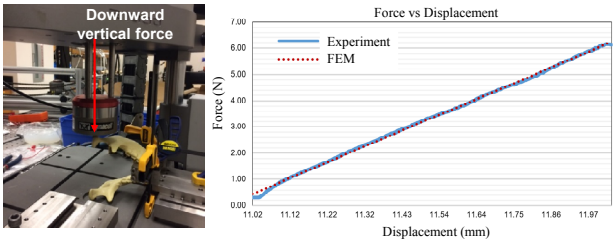

(a) (b)

Fig. 2. (a) Experimental setup for artificial mandible using Instron testing machine; (b) force-displacement graph by lateral (y-directional) incremental force.

2.1 Static analysis of the human mandible

First, we used an artificial mandible from 3B Scientific [20] since human mandible samples could not be acquired. A displacement in lateral direction (*y*-direction) by the load in the same direction was compared between experimental loading and FE analysis (Fig. 2). In Fig. 2, an Instron testing machine applied loading on the lateral surface of the condyle to initiate bending of the mandible fixed at the center (Fig. 2(a)). The force displacement data was measured and shown in Fig. 2(b), where a stiffness of 5.75 N/mm is found.

Identical loading conditions were simulated in the FE model with the following Young's moduli provided by the manufacturer [20]: 1.5 GPa, 100 MPa, and 1.5 GPa for cortical bone, trabecular bone, and dentin, respectively. The static analysis yielded a maximum downward displacement of 0.881 mm, about 12 % different from the experimental condition. Considering measurement error and the possible delicate difference of material properties from the manufacturer [20], this displacement is acceptable.

We further conducted a static analysis using realistic mandible properties to observe maximum displacement and stress to verify these results to the values found in literature. In this paper, the mechanical properties (Young's modulus) of the human mandible were chosen as 100 MPa and 16 GPa for the trabecular and cortical bone, respectively (Table 1). These fall within a range of values found in literature: 13.7~17.5 GPa for the cortical bone [18, 21], and 62~114 MPa for the trabecular bone [21-24].

In this paper, sliding boundary conditions were applied to the condyle to represent the temporomandibular joint (TMJ) for computational efficiency, and on the sagittal plane to represent symmetry. Additionally, a displacement boundary condition restricting motion along the z-axis was applied on the first and second molar to simulate teeth contact during mastication. Fig. 3(a) shows the boundary conditions imposed on the FE model.

Table 1. Material properties of the finite element model for the mandible.

Material	Young's modulus	Poisson's ratio
Cortical	16 GPa	0.3
Trabecular	100 MPa	0.3
Dentin	17.6 GPa [25]	0.25

Table 2. Magnitude and direction of the primary mastication muscles [15].

Muscle	Portion	F_m (N)	F_{mx} (N)	F_{my} (N)	F_{mz} (N)
Temporalis	Anterior	158.00	6.95	-23.54	-156.10
	Middle	95.00	-47.50	-21.00	-79.52
	Posterior	75.00	-64.15	-15.60	-35.55
	Sum	296.84	-104.67	-60.14	-271.17
Masseter		190.40	79.78	-39.41	-168.50
Medial pterygoid		174.80	65.03	84.95	-138.27
Lateral pterygoid		66.90	50.64	42.15	11.64

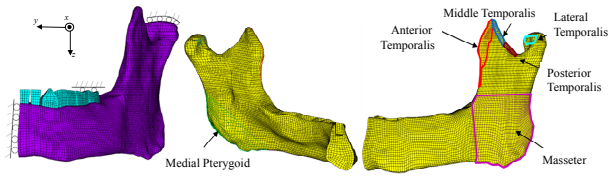

(a) (b) (c)

Fig. 3. FE model with (a) boundary conditions; (b) and (c) various mandibular muscles responsible for closing.

To replicate a masticatory cycle, the maximum forces for the masseter, temporalis, medial pterygoid, and lateral pterygoid from Table 2 were applied on the mandible at their respective areas of insertion. In Table 2, each of the maximum force during isometric contraction was defined as F_m, and its directional components were indicated as F_{mx}, F_{my}, and F_{mz}. These forces were applied on the corresponding parts of mandible as shown in Figs. 3(b) and (c). The muscles are assumed to exhibit bilateral behavior.

The analysis result shows that the maximum lateral displacement is 0.37 mm outwards for the half mandible (Fig. 4(a)), or a total lateral displacement of 0.74 mm. This value is within the 0.46 to 1.06 mm range described in the literature [19, 26]. In Fig. 4(b), the von Mises stress ranges from 5 to 94.6 MPa for static loading. A concentration of stress observed on the contour plot, indicated by the red circle, was neglected since it is a result of the loading of the mandibular muscles and the sharp contour of the geometry. The von Mises stress range for the rest of the mandible fell in a range found in literature (2 to 53.4 MPa [16]).

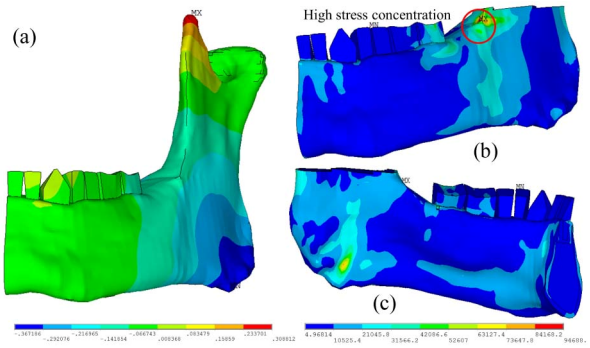

Fig. 4. FE model with (a) boundary conditions; (b) and (c) various mandibular muscles responsible for closing.

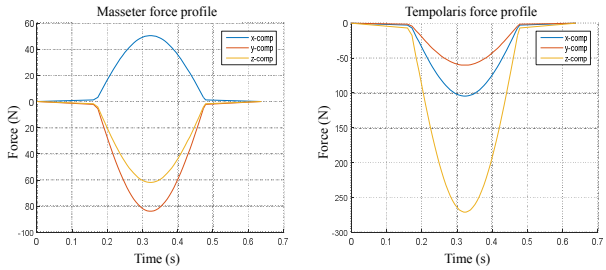

Fig. 5. Directional force profiles for masseter (left) and temporalis (right) muscles.

2.2 Dynamic analysis of the human mandible

Following the static analysis, a dynamic analysis was run to predict dynamic mandibular deformation and explore energy harvesting capabilities. Based on electromyography (EMG) records from muscles of mastication acting on the mandible [15, 27], the force profile was approximated as a half cycle of a sine wave with a non-zero slope during inactive period of muscle force to prevent unrealistic jumps of velocity/acceleration, with peaks obtained from the maximum forces for each muscle in Table 2 and a frequency of 1.57 Hz to represent chewing [28] (Fig. 5). Boundary conditions were applied on the mandible in the same manner as done in the static analysis. The transient analysis in this section considered only the masseter and temporalis muscles, the two main muscles acting on the mandible responsible for closing movements.

Similar to the static analysis, the maximum displacement and stress were observed on the side of the mandible. The lateral displacement had a peak of 0.54 mm outwards direction, shown in Fig. 6(a) (circled area for maximum displacement). From this analysis, the areas that experienced more deformation were taken into consideration for possible placement locations of the harvester. Ignoring the high stress concentration due to sharp geometry, the von Mises stress ranged from 9-36 MPa (Fig. 6(b)).

3. Design of the piezoelectric energy harvester

The harvester design and location was carefully determined

Table 3. MFC piezoelectric properties.

$S_{11} = S_{22}$ ($\times 10^{-9}$m^2/N)	S_{33}	S_{44}	$S_{55} = S_{66}$	S_{12}	$S_{13} = S_{23}$
0.065	0.034	0.165	0.173	-0.205	-0.0106
$d_{33}{}^0$ ($\times 10^{-10}$m/V)	$d_{31}{}^0$	-	ε_{11}	ε_{22}	ε_{33}
-1.53	4.34	-	712	1.7	737

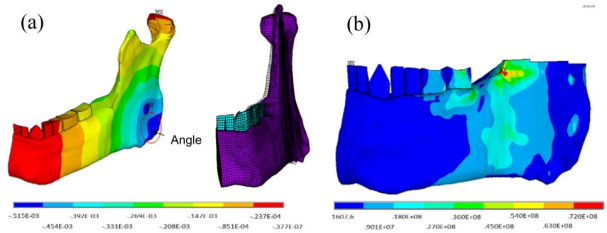

Fig. 6. FE analysis of the mandible, transient loading by two muscles: (a) Maximum lateral displacement at time at t = 0.33 s (m); (b) von Mises stress contour at time of peak magnitude of the mandible (Pa).

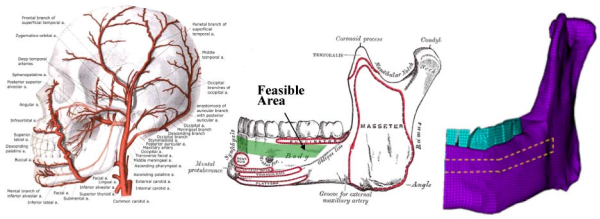

Fig. 7. (a) Nerves and blood vessels surrounding the mandible; (b) diagram showing feasible areas to place the harvester (marked by green box); (c) position of harvester on mandible (dashed yellow line).

based on the information from the FE analysis as well as mandibular anatomy and patient comfort. There are numerous factors that affect the power output of a harvester, such as the type and shape of the piezoelectric material, position of the harvester on the energy source, and configuration of the piezoelectric material on the harvester. In Fig. 7(b) we delineated possible placement of the harvesting device on the posterior body of the mandible, indicated by the green box, which is free of anatomical constraints (Fig. 7(a)). In this paper, the harvester location along the surface of the posterior body highlighted with a rectangular shape as shown in Fig. 7(c) was investigated.

To ensure biocompatibility and the desired structural flexibility for an *in vivo* energy harvesting application, macro fiber composite (MFC, Smart Material Corporation) [29] incorporated with a titanium substrate was selected as the piezoelectric material. MFC with the dimensions, 37 × 10 × 0.3 mm^3 (active area 28 × 8 mm^2), was selected to fit the area in Fig. 7(c). The compliance coefficients (S), the piezoelectric strain coefficients (d: d_{31} and d_{33}), and relative permittivity (ε) are defined in Table 3.

3.1 Selection of harvester design

For this study we selected a unimorph (single MFC layer)

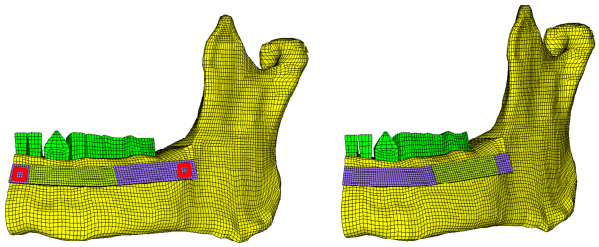

Fig. 8. Locations for MFC placement along titanium substrate.

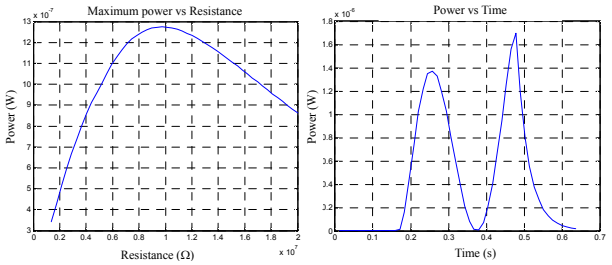

(a) (b)

Fig. 9. (a) Maximum power output as a function of resistance; (b) plot of power (W) vs time (s) for harvester configuration.

along with a substrate to minimize patient discomfort. A transient analysis of the mandible with the harvester was performed to compare the power level between two different harvester locations as shown in Fig. 8. Three titanium screws (red rectangle locations in Fig. 8 (left) were used to fix the substrate to the mandible (two at each end, and one at the center).

The FE analysis yielded larger electrical output (open circuit voltage) for the first location - the second location was not particularly conducive to capture strain energy due to smaller bending stress. For the first location, a study was performed to determine the optimal resistance for maximum power output (9.72×10^6 Ohms). In Fig. 9(a), the maximum average power was found to be 1.28 μW. Fig. 9(b) shows the time history of power with the optimal resistance value with peak power of 1.7 μW.

4. Experimental power evaluation

4.1 Design of mandibular loading apparatus

We chose two representative mandibular muscle forces (temporalis and masseter, see Sec. 2.2) whose dynamic behaviors were realized by a unique lever apparatus. For this apparatus, the driving force from a controlled linear actuator was transmitted to the mandible via a coupled lever, rope and pulley system (Fig. 10).

The levers receive the force from the actuator and amplifies it corresponding the mechanical advantage needed to properly represent the masseter and temporalis muscular forces as follows:

$$\frac{F_0}{F_i}=\frac{d_i}{d_0}. \tag{1}$$

Table 4. Lever design parameters and descriptions.

Parameter	Description
F_T	Force on temporalis
F_M	Force on masseter
F_i	Force of the actuator
d_o^i	Distance from fulcrum to force on temporalis
d_o^M	Distance from fulcrum to force on masseter
d_i	Distance from the fulcrum to the force of the actuator

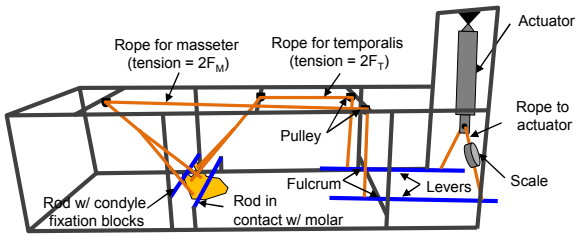

(a)

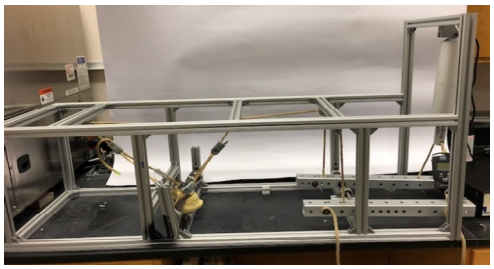

(b)

Fig. 10. (a) Components in test apparatus; (b) whole view of the testing apparatus.

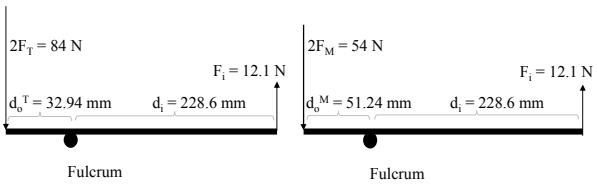

Fig. 11. Lever design for the temporalis (left) and masseter (right) muscles.

F_o and F_i represent the output and input forces, d_i and d_o represent the distances from the fulcrum to the input and output force, respectively (see Table 4 for a detailed description of lever design parameters). Because the material properties of the artificial mandible used in this paper are lower than a realistic mandible, the magnitude of the muscular forces was scaled down by a factor of 7 to maintain consistency with the deformation level in Fig. 6(a). The calculation of the magnitudes of the masseter and temporalis muscles is graphically shown in Fig. 11. The actuator force was controlled by using a function generator that provides a continuous sinusoidal function at 1.57 Hz. The ropes coupled to the levers achieve the desired force profile (Fig. 5) since they only transmit force

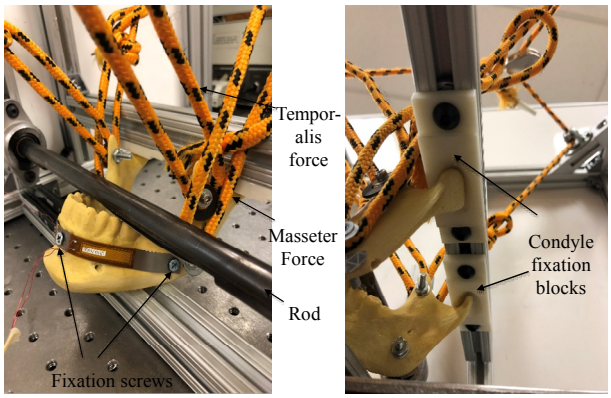

Fig. 12. View of ropes representing masseter and temporalis forces (left); view of condyle fixation blocks (right).

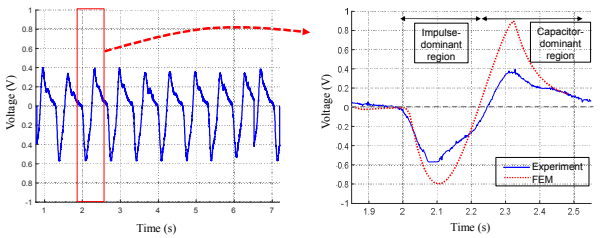

Fig. 13. Open-circuit voltage (Voltage (V) vs. time) measured from FEA (blue) and experiment (red) via manual activation of the lever.

while in tension.

To imitate the boundary conditions imposed on the FE model (Fig. 3), two blocks with an indentation to match the shape of the condyles were 3D printed and fixed to the frame of the apparatus (Fig. 12). A rod was placed across the molars to fix vertical displacement of the mandible. The ends of ropes were fastened onto the mandible with screws to mimic mandibular loading. During the load testing, the dynamic force profile was monitored by a digital scale inserted between the ropes attached to the lever (Fig. 10) and lateral displacement of the mandible is measured via laser vibrometer.

The harvesting device was attached to the mandible using screws (Fig. 12) that are commonly used in mandibular surgical procedures [30, 31]. While the dynamic loading was applied, the open-circuit voltage of one MFC was measured using an oscilloscope, and a peak-to-peak voltage of about 1.0 V was measured (Fig. 13). The peak-to-peak voltage predicted from the FEA was 1.7 V.

Recent advancements in self-powering DBS systems have yielded lower power requirements, typically ranging between 7.4~132 μW [32-35]. The parametric study on the resistor in Fig. 9(a) shows that our proposed prototype can offer an average power, $P_{ave} = 1/T \times \int P(t)dt = 1/T \times \int \{V^2(t)/R\}dt$, up to 1.27 μW, where T is the time interval for integration. While the power output is lower than required, it can be further amplified by multilayered MFC design or developing an optimal circuit.

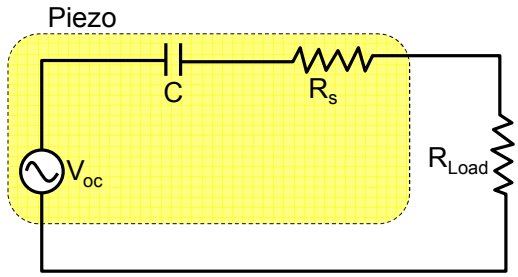

Fig. 14. Equivalent circuit of PZT.

4.2 Discussion

The results of the experiment offer significant insight into the energy harvesting capabilities under low excitation frequencies. The double-peak voltage response (with negative and positive peaks) can be explained using the equivalent circuit of PZT in Fig. 14. The double-peak phenomenon is caused by a nonzero phase shift $\phi = \tan^{-1}(-1/\omega\tau) = \tan^{-1}(-1/\omega RC) \cong -34$ degrees contributed by a small excitation frequency $\omega = 1.57 \times 2\pi$ (rad/s), when $R = 9.72 \times 10^6$ (Ohm) and $C = 15 \times 10^9$ (F). This means the phase of the current is faster than that of source voltage (V_{cc}) by 34 degrees as observed in the negative maximum value at $t \cong 2.1$ s (Fig. 13). At $t \cong 2.24$ s, the current reached zero before V_{cc}, but the increasing V_{cc} caused the current to also increase, resulting in a positive peak current at $t \cong 2.33$ s. Because the voltage phase at the resistive load is equal to the current phase in the series equivalent circuit (Fig. 14), the double-peak voltage response appeared at the resistive load. At the beginning of the capacitor dominant region (after $t \cong 2.33$ s in Fig. 13), there is no input force. Therefore, most of the energy stored in the piezoelectric capacitor (C) is transferred to the resistive load up to the end of cycle (2.55 s).

The discrepancy between simulation and experiment is primarily due to the loosening of rope and the corresponding tension reduction that can decrease the measured peak-to-peak voltage, even though we could obtain very similar voltage waveforms (Fig. 13). Furthermore, the voltage output is sensitive to small changes in positioning of the mandible under the applied boundary conditions. Future efforts can be made regarding methods to minimize the amount of force transmission loss (e.g. using metal wire rope) and robust fixing conditions for the mandible. A possible implementation of using the power in this study is by integrating with a power management integrated circuit (PMIC) that efficiently accumulates a micro power (μW) and periodically charges a storage device for DBS system [36]. An additional power line would be required from the storage device to the DBS system.

5. Conclusions

This study investigated the feasibility of a piezoelectric energy harvester implanted on the human mandible to provide

power to a DBS device, by comparing simulation (finite element method) and experiment conducted via a uniquely designed testing apparatus that mimics the mastication forces. We analyzed the output voltage waveform, found identical between FEA and experiment, and discussed a method to use the power for DBS. While power generation of the device is low to power a commercial DBS, further investigation is underway to improve the experiments and increase power output of the device.

Acknowledgments

This research was supported by UMB-UMBC Research and Innovation Partnership Grant Program (2016~2017). The authors thank Mr. Danny Joh and Mr. Poojan Shah for assisting in the test setup.

Nomenclature

C	: Capacitance
d_{ii}^0	: Piezoelectric strain coefficients
d	: Distance
ε	: Relative permittivity
F	: Force
S	: Compliance coefficient
ϕ	: Phase shift
ω	: Frequency
V_{cc}	: Source voltage

References

[1] Deep Brain Stimulation, *https://en.wikipedia.org/wiki/Deep_brain_stimulation*.

[2] K. Fakhar, E. Hastings, C. R. Butson, K. D. Foote, P. Zeilman and M. S. Okun, Management of deep brain stimulator battery failure: Battery estimators, charge density, and importance of clinical symptoms, *PLoS One*, 8 (3) (2013) e58665.

[3] M. A. Karami and D. J. Inman, Powering pacemakers from heartbeat vibrations using linear and nonlinear energy harvesters, *Appl. Phys. Lett.*, 100 (4) (2012) 1-5.

[4] M. H. Ansari and M. A. Karami, Piezoelectric energy harvesting from heartbeat vibrations for leadless pacemakers, *J. Phys. Conf. Ser.*, 660 (1) (2015) 012121.

[5] G. Sahara, W. Hijikata, K. Tomioka and T. Shinshi, Implantable power generation system utilizing muscle contractions excited by electrical stimulation, *Proc. Inst. Mech. Eng. Part H J. Eng. Med.*, 230 (6) (2016) 569-578.

[6] B. E. Lewandowski, K. L. Kilgore and K. J. Gustafson, Design considerations for an implantable, muscle powered piezoelectric system for generating electrical power, *Ann. Biomed. Eng.*, 35 (4) (2007) 631-641.

[7] R. Yang, Y. Qin, C. Li, G. Zhu and Z. Lin Wang, Converting biomechanical energy into electricity by a muscle-movement-driven nanogenerator, *Nanoletters*, 9 (3) (2009) 1201-1205.

[8] T. Starner, Human-powered wearable computing, *IBM Systems Journal*, 35 (1996) 618-629.

[9] J. W. Sohn, S. B. Choi and D. Y. Lee, An investigation on piezoelectric energy harvesting for MEMS power sources, *Proc. Inst. Mech. Eng. Part C J. Mech. Eng. Sci.*, 219 (4) (2005) 429-436.

[10] G.-T. Hwang, Y. Kim, J.-H. Lee, S. Oh, C. K. Jeong, D. Y. Park, J. Ryu, H. Kwon, S.-G. Lee, B. Joung, D. Kim and K. J. Lee, Self-powered deep brain stimulation via a flexible PIMNT energy harvester, *Energy & Environmental Science*, 8 (9) (2015) 2677-2684.

[11] M. Hosain, A. Kouzani, M. Samad and S. Tye, A miniature energy harvesting rectenna for operating a head-mountable deep brain stimulation device, *IEEE Access*, 3 (2015) 223-234.

[12] L. Beker, A. Benet, A. T. Meybodi, B. Eovino, A. P. Pisano and L. Lin, Energy harvesting from cerebrospinal fluid pressure fluctuations for self-powered neural implants, *Biomedical Microdevices*, 19 (2) (2017).

[13] A. Delnavaz and J. Voix, Flexible piezoelectric energy harvesting from jaw movements, *Smart Materials and Structures*, 23 (10) (2014) 105020.

[14] M. S. Commisso, J. Martínez-Reina, J. Ojeda and J. Mayo, Finite element analysis of the human mastication cycle, *J. Mech. Behav. Biomed. Mater.*, 41 (2015) 23-35.

[15] J. M. Reina, J. M. García-Aznar, J. Domínguez and M. Doblaré, Numerical estimation of bone density and elastic constants distribution in a human mandible, *J. Biomech.*, 40 (4) (2007) 828-836.

[16] P. Bujtár, G. K. B. Sándor, A. Bojtos, A. Szűcs and J. Barabás, Finite element analysis of the human mandible at 3 different stages of life, *Oral Surgery, Oral Med. Oral Pathol. Oral Radiol. Endodontology*, 110 (3) (2010) 301-309.

[17] A. Szucs, P. Bujtar, G. K. Sandor and J. Barabas, Finite element analysis of the human mandible to assess the effect of removing an impacted third molar, *J. Can. Dent. Assoc.*, 76 (2009) 1-7.

[18] E. Tanaka, K. Tanne and M. Sakuda, A three-dimensional finite element model of the mandible including the TMJ and its application to stress analysis in the TMJ during clenching, *Med. Eng. Phys.*, 16 (4) (1994) 316-322.

[19] A. H. Choi, B. C. Ben-Nissan and R. C. Conway, Three-dimensional modelling and finite element analysis of the human mandible during clenching, *Aust. Dent. J.*, 50 (1) (2005) 42-48.

[20] 3B Scientific, *https://www.a3bs.com/*.

[21] P. Xin, P. Nie, B. Jiang, S. Deng, G. Hu and S. G. F. Shen, Material assignment in finite element modeling, *J. Craniofac. Surg.*, 24 (2) (2013) 405-410.

[22] É. Lakatos, L. Magyar and I. Bojtár, Material properties of the mandibular trabecular bone, *J. Med. Eng.*, 2014 (2014) 1-7.

[23] A. M. O'Mahony, J. L. Williams, J. O. Katz and P. Spencer, Anisotropic elastic properties of cancellous bone

from a human edentulous mandible, *Clin. Oral Implants Res.*, 11 (5) (2000) 415-421.
[24] J. B. Brunski, Mechanical properties of trabecular bone in the human mandible: Implications for dental implant treatment planning and surgical placement, *J. Oral Maxillofac. Surg.*, 57 (6) (1999) 706-708.
[25] S. Kayumi, Y. Takayama, A. Yokoyama and N. Ueda, Effect of bite force in occlusal adjustment of dental implants on the distribution of occlusal pressure: Comparison among three bite forces in occlusal adjustment, *Int. J. Implant Dent.*, 1 (1) (2015) 14.
[26] T. W. Korioth, A. G. Hannam and J. D. Res, Deformation of the human mandible during simulated tooth clenching, *J Dent Res.,* 73 (1) (1994) 56-66.
[27] W. L. Hylander, *Functional Anatomy and Biomechanics of the Masticatory Apparatus*, Quintessence Publishing Company, Batavia, USA (2006).
[28] J. M. Po, J. A. Kieser, L. M. Gallo, A. J. Tesenyi, P. Herbison and M. Farella, Time-frequency analysis of chewing activity in the natural environment, *J. Dent. Res.*, 90 (10) (2011) 1206-1210.
[29] Smart Material Corp., *https://www. smart-material.com*.
[30] M. M. Omezli, D. Torul, M. E. Polat and E. Dayi, Biomechanical comparison of osteosynthesis with poly-L-lactic acid and titanium screw in intracapsular condylar fracture fixation: An experimental study, *Niger. J. Clin. Pract.*, 18 (5) (2015) 589-93.
[31] S. Miyawaki, I. Koyama, M. Inoue, K. Mishima, T. Sugahara and T. Takano-Yamamoto, Factors associated with the stability of titanium screws placed in the posterior region for orthodontic anchorage, *Am. J. Orthod. Dentofac. Orthop*., 124 (4) (2003) 373-378.
[32] A. Haddock, K. T. Mitchell, A. Miller, J. L. Ostrem, H. J. Chizeck and S. Miocinovic, Automated deep brain stimulation programming for tremor, *IEEE Transactions on Neural Systems and Rehabilitation Engineering*, 26 (8) (2018) 1618-1625.
[33] S. Little et al., Adaptive deep brain stimulation in advanced Parkinson disease, *Annals of Neurology*, 74 (3) (2013) 449-457.
[34] J. Lee, H. Rhew, D. Kipke and M. Flynn, A 64 channel programmable closed-loop neurostimulator with 8 channel neural amplifier and logarithmic ADC, *IEEE Journal of Solid-State Circuits*, 45 (9) (2010) 1935-1945.
[35] R. Cubo, M. Fahlström, E. Jiltsova, H. Andersson and A. Medvedev, Calculating deep brain stimulation amplitudes and power consumption by constrained optimization, *Journal of Neural Engineering*, 16 (1) (2019) 016020.
[36] S. Boisseau, P. Gasnier, M. Gallardo and G. Despesse, Self-starting power management circuits for piezoelectric and electret-based electrostatic mechanical energy harvesters, *J. of Physics: Conference Series*, 476 (2013) 012080.

Richard Fan received an M.S. from the University of Maryland, Baltimore County (UMBC) in 2018. He is currently an Engineer at the Department of Defense where his main specialty is finite element analysis of highly dynamic events. His research interest includes biomedical application of a piezoelectronic energy harvesting device.

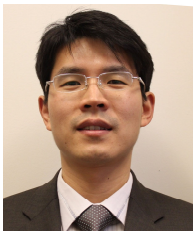

Soobum Lee received the Ph.D. in Mechanical Engineering, Korea Advanced Institute of Science and Technology (KAIST), Daejeon, South Korea, in 2007. He is currently an Assistant Professor with the University of Maryland Baltimore County, Baltimore MD, USA. His main research interests include energy harvesting device design, structural topology optimization, and robust and reliability-based design optimization.

Hyun Jun Jung received the Bachelor of Engineering (electrical) from Seoul National University of Science and Technology, Seoul, South Korea in 2012. He received his Ph.D in Electrical Engineering in Hanyang University, Seoul, South Korea, in 2017 and then he started a postdoctorate at the University of Maryland Baltimore County, Baltimore, USA. His research interests include design of piezoelectric energy harvesting device, low power management circuit, and piezoelectric transformer.

Mary Anne Melo earned her D.D.S. in 2000 from the University of Fortaleza in Ceara, Brazil, and her M.Sc. and Ph.D. in Dentistry from the Federal University of Ceara in 2012 for her work on nanotechnology-based restorative materials for dental caries management. Her primary research interests are anticaries strategies to reduce biofilm growth and acid production.

Radi Masri is an Associate Professor at the School of Dentistry and School of Medicine, University of Maryland. He is the Program Director of the Advanced Education Program in Prosthodontics and the Director of Research and Discovery Division at the Department of Advanced Oral Sciences and Therapeutics.